Proton-Coupled Electron Transfer in Tyrosine and a β-Hairpin Maquette: Reaction Dynamics on the Picosecond Time Scale

ARTICLE *in* THE JOURNAL OF PHYSICAL CHEMISTRY B · DECEMBER 2014

Impact Factor: 3.3 · DOI: 10.1021/jp510171z · Source: PubMed

THE JOURNAL OF PHYSICAL CHEMISTRY B

Article

pubs.acs.org/JPCB

Proton-Coupled Electron Transfer in Tyrosine and a β-Hairpin Maquette: Reaction Dynamics on the Picosecond Time Scale

Cynthia V. Pagba,[†] San-Hui Chi,[‡] Joseph Perry,[‡] and Bridgette A. Barry*,[†]

[†]School of Chemistry and Biochemistry, Petit Institute for Bioengineering and Bioscience, and [‡]Center of Organic Photonics and Electronics, Georgia Institute of Technology, Atlanta, Georgia 30332, United States

Supporting Information

ABSTRACT: In proteins, proton-coupled electron transfer (PCET) can involve the transient oxidation and reduction of the aromatic amino acid tyrosine. Due to the short life time of tyrosyl radical intermediates, transient absorption spectroscopy provides an important tool in deciphering electron-transfer mechanisms. In this report, the photoionization of solution tyrosine and tyrosinate was investigated using transient, picosecond absorption spectroscopy. The results were compared to data acquired from a tyrosine-containing β-hairpin peptide. This maquette, peptide A, is an 18-mer that exhibits π−π interaction between tyrosine (Y5) and histidine (H14). Y5 and H14 carry out an orthogonal PCET reaction when Y5 is oxidized in the mid-pH range. Photolysis of all samples (280 nm, instrument response: 360 fs) generated a solvated electron signal within 3 ps. A signal from the S_1 state and a 410 nm signal from the neutral tyrosyl radical were also formed in 3 ps. Fits to S_1 and tyrosyl radical decay profiles revealed biphasic kinetics with time constants of 10−50 and 400−1300 ps. The PCET reaction at pH 9 was associated with a significant decrease in the rate of tyrosyl radical and S_1 decay compared to electron transfer (ET) alone (pH 11). This pH dependence was observed both in solution and peptide samples. The pH 9 reaction may occur with a sequential electron-transfer, proton-transfer (ETPT) mechanism. Alternatively, the pH 9 reaction may occur by coupled proton and electron transfer (CPET). CPET would be associated with a reorganization energy larger than that of the pH 11 reaction. Significantly, the decay kinetics of S_1 and the tyrosyl radical were accelerated in peptide A compared to solution samples at both pH values. These data suggest either an increase in electronic coupling or a specific, sequence-dependent interaction, which facilitates ET and PCET in the β hairpin.

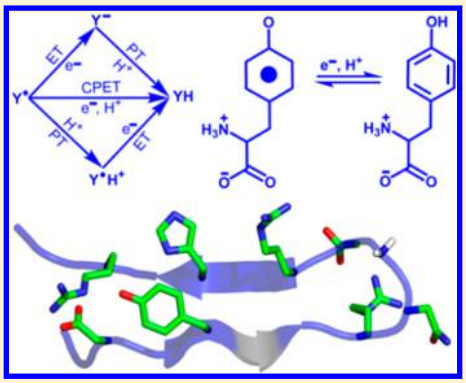

Biological electron-transfer (ET) reactions are mediated by tunneling with rates that decrease exponentially with distance. To accelerate ET reactions into a physiologically relevant time frame, redox-active cofactors can be transiently oxidized and reduced in a hopping mechanism, which defines a radical or charge transport pathway.[1] The aromatic amino acids tyrosine and tryptophan serve as essential redox-active cofactors in a variety of important biological processes (reviewed in ref 2). For example, tryptophan side chains play crucial roles in picosecond ET in DNA photolyase.[3] In addition, tyrosine-based charge transfer is known to play an essential role in several enzymes, including photosystem II (PSII) and ribonucleotide reductase (see refs 4−9 and refs therein). PSII has two redox-active tyrosines, YZ (Y161 of the D1 subunit) and YD (Y160 of the D2 subunit), which are oxidized via a light-generated, high potential chlorophyll cation radical. Each of these redox-active tyrosines interacts through a hydrogen bond with a protonable histidine side chain.[10] The two tyrosines have different protein environments and distinct roles in electron transfer. These distinctions in noncovalent and covalent interactions distinguish the two tyrosines and must be functionally important, but the mechanism is not yet understood (reviewed in ref 8).

$$k_{ET} = \left(\frac{\pi}{\hbar^2 \lambda k_B T}\right)^{1/2} \cdot |V_{DA}|^2 \cdot e^{-\frac{(\Delta G^\circ + \lambda)^2}{4\lambda k_B T}} \quad (1)$$

At pH values above the phenolic pK_a (10),[11] oxidation of tyrosine results in the formation of a neutral tyrosine radical in an ET reaction (Figure 1A). As described in the Marcus equation for outer-sphere electron transfer (eq 1), ET rates depend on driving force (ΔG°, reorganization energy (λ), and electronic coupling between donor (D) and acceptor (A) (V_{DA}).[2,12] The midpoint potential of tyrosine is pH dependent and described by the Nernst equation.[13] Electronic coupling has been shown to exhibit exponential dependence on the donor−acceptor distance (R_{DA}) with a β value (eq 2)[1] that is influenced by protein structure.[14] In eq 2, V_0 represents maximal electronic coupling.

Special Issue: Photoinduced Proton Transfer in Chemistry and Biology Symposium

Received: October 8, 2014
Revised: November 11, 2014
Published: December 1, 2014

dx.doi.org/10.1021/jp510171z | J. Phys. Chem. B 2015, 119, 2726−2736

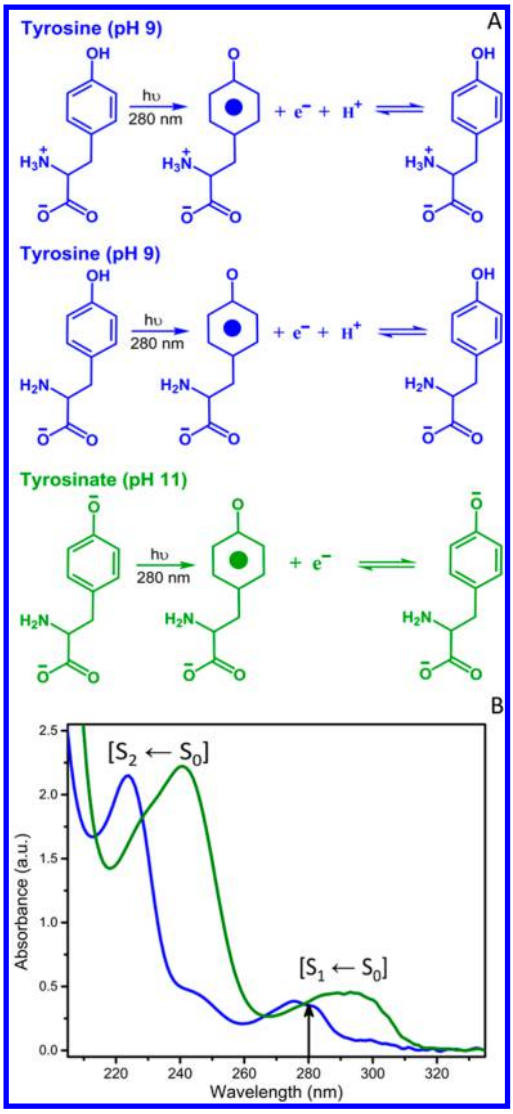

Figure 1. Structures and reactions of tyrosine at pH 9 (blue) and tyrosinate at pH 11 (green) following excitation with a 280 nm pulse. (A) At pH 9, the sample is a mixture of zwitterionic and anionic forms due to protonation of the terminal amino group (pK_a ~9.3). Photolysis at pH 9 causes a PCET reaction by breaking the OH bond to produce a neutral tyrosyl radical and a solvated electron. Photolysis at pH 11 causes an ET reaction to produce a neutral tyrosyl radical and a solvated electron. (B) Steady state absorption spectra of a 1 mM solution derived from tyrosine (blue) or tyrosinate (green) in 5 mM borate−NaOH aqueous buffer and measured in a 2 mm quartz cuvette. The arrow indicates the 280 nm excitation wavelength used in the transient absorption measurements.

$$|V_{DA}|^2 = |V_0|^2 \cdot e^{(-\beta R_{DA})} \quad (2)$$

In the mid-pH range, tyrosine retains its phenolic proton (pK_a 10). When tyrosine (Figure 1A) is oxidized, a neutral tyrosyl radical is formed, due to the low pK_a of the radical's phenolic oxygen (≤0).[15] Therefore, oxidation of tyrosine results in a proton-coupled ET (PCET) reaction. In this paper, we use PCET to refer to any reaction in which an electron and proton are transferred, regardless of mechanism.[16] When PCET occurs, the proton- and electron-transfer reactions may be collinear or orthogonal, in which an electron and proton are transferred to different acceptors (Figure 1A) (reviewed in ref 17). Proton-transfer reactions occur over short distances, and therefore, the mechanism of PCET depends on short-range, noncovalent interactions in proteins. Theoretical treatments have been developed to predict the rates of PCET reactions.[18]

Mechanisms of tyrosyl radical formation and decay in complex proteins, such as PSII, have been investigated and discussed.[16] However, the complexity of large biological systems can complicate interpretation. To define a reaction mechanism in a more structurally tractable system, a variety of approaches have been employed. Tyrosyl radicals have been generated in aqueous solutions of tyrosine or tyrosinate by nanosecond UV pulses or by pulse radiolysis. To measure the reaction rate, the decay of the neutral radical was monitored by its narrow absorption band at 410 nm.[19,20] Studies of tyrosyl radical reaction rates have been reported in tyrosine-containing dipeptides using a similar method.[21] Tyrosyl radicals have also been generated in more complex model compounds using ruthenium or rhenium photosensitizers, which oxidize tyrosine and tyrosinate from either the excited or ground state (reviewed in ref 16). For example, this approach has been used to generate tyrosyl radicals in a covalently linked tyrosine−ruthenium−tris−bipyridine complex.[22,23] Ruthenium and rhenium sensitizers were covalently linked to the copper-containing protein azurin; aromatic amino acid radicals were generated, and the formation and decay kinetics were then determined.[24,25] Ruthenium photosensitizers were also used to study the kinetics of tyrosyl radical formation and decay in the model peptide α3, which forms an α-helical bundle.[26]

A β-hairpin tyrosine-containing model has also been described; it is an 18-mer peptide that has been designed *de novo* and is inspired by PSII.[27,28] Peptide A is an 18-mer and contains a single tyrosine (Y5) and cross-strand histidine (H14). The NMR structure of peptide A was determined and showed that the peptide folds to form a β-hairpin in which the tyrosine and histidine are $\pi-\pi$ stacked in a cross-strand interaction. Electrochemical evidence indicated that this peptide maquette exhibits an orthogonal PCET reaction between histidine and tyrosine in the mid-pH range.[27] There is no evidence for a direct hydrogen bond between tyrosine and histidine, implying the participation of hydrogen-bonded water in the PCET reaction.

In proteins such as DNA photolyase and PSII, aromatic amino acids are oxidized and/or reduced on the picosecond to nanosecond time scale.[3,29] Little is known concerning the effect of covalent and noncovalent interactions on such rapid reactions. As mentioned above, nanosecond UV photolysis, which forms a tyrosyl radical in the excited state, leads to ionization of tyrosine or tyrosinate. However, to probe reaction dynamics on the picosecond time scale, ultrafast UV pulses are necessary. Picosecond experiments, using 266 nm photolysis, have been reported for phenol and phenolate. The absorption bands of the S_1 excited state, the neutral radical, and the solvated electron were assigned.[30,31] Less is known about picosecond dynamics in tyrosine and tyrosinate, which are less soluble compared to phenol and phenolate.

Here, we report picosecond time-resolved experiments using a 280 nm ultrafast photolysis pulse to photooxidize tyrosine or tyrosinate in a dilute aqueous solution; the photoionization reaction in these two samples is associated with either a PCET or ET reaction, respectively. The results are compared with the photooxidation of tyrosine or tyrosinate in the peptide A maquette. The kinetic results define a pH-dependent mechanism of tyrosyl radical decay and show that covalent

dx.doi.org/10.1021/jp510171z | J. Phys. Chem. B 2015, 119, 2726−2736

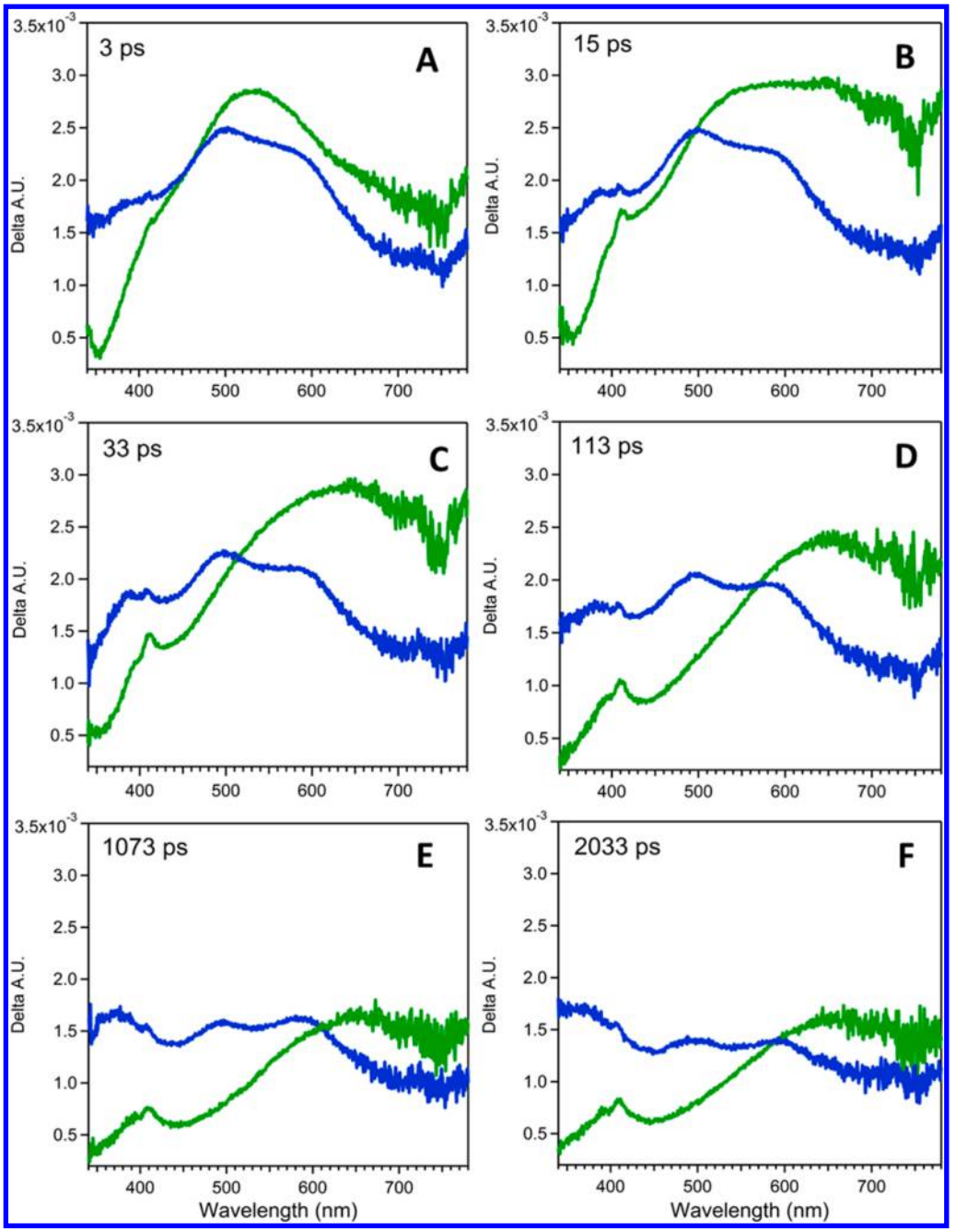

Figure 2. Spectral slices derived from either tyrosine at pH 9 (blue) or tyrosinate at pH 11 (green) at the time points indicated. Analyte concentration, 1 mM; buffer, 5 mM borate−NaOH. See Materials and Methods for more information.

and specific, noncovalent interactions in the β-hairpin accelerate early events in ET and PCET.

MATERIALS AND METHODS

Tyrosine and boric acid were purchased from Sigma (St. Louis, MO; 99.9% purity). Peptide A (IMDRYRVRNGDRIHIRLR) was synthesized by solid state synthesis and was obtained from Genscript (Piscataway, NJ; >95% purity).[27,28]

Transient absorption spectra[32] were acquired with a pump-white light continuum probe spectroscopy system (Ultrafast Systems, Helios). The measurement system consists of a regeneratively amplified titanium sapphire laser (Solstice, Spectra-Physics, 800 nm, 3.7 W average power, 100 fs pulse width, 1 kHz repetition rate) and a computer-controlled optical parametric amplifier (OPA) (Spectra-Physics, TOPAS, wavelength range: 266−2600 nm, pulse width: ∼75 fs $HW_{1/e}$) that is pumped by the amplified laser. The 280 nm photolysis pulse was generated using the fourth-harmonic output of the OPA. A white light continuum (WLC) probe beam with a spectral range from 350 to 750 nm was generated by focusing less than 5% of the 800 nm amplified beam into a CaF_2 crystal. The probe signal was collected using a fiber optic cable coupled to a spectrometer with a multichannel CMOS sensor and with a spectral range of 300−900 nm. The maximum time delay was 3.2 ns. The pump beam was chopped at 500 Hz to obtain the WLC spectrum alternately without pump and with the 280 nm pump. These data were used to calculate the transient spectra, represented as a change in optical density or absorbance units

dx.doi.org/10.1021/jp510171z | J. Phys. Chem. B 2015, 119, 2726−2736

(A.U.). Each transient spectrum at a given time delay was averaged for 4 s. A chirp correction function for the WLC probe was determined using the coherent artifact of the organic solvent tetrahydrofuran and was applied to all transient spectra.[33] The optical path length of the quartz cuvette was 2 mm. The excitation pulse energy was 2−3 μJ. The averaged beam waist ($HW_{1/e}$) was ∼160 μm for the pump and ∼80 μm for the WLC. In 2 mm path-length cuvettes, the solutions were stirred throughout data acquisition and had an OD_{280} of 0.30−0.50. The tyrosyl radical was not generated at pH values less than 9. Steady state absorption spectra, recorded before and after the ultrafast measurements on a Shimadzu UV-3101PC spectrophotometer, showed no significant change (Figure S1, Supporting Information (SI)). As assessed by the 410 nm signal amplitude at 3 ps, the radical yield was 0.21−0.24%. It has been reported previously that triplet state signals are not expected in oxygenated samples.[19]

RESULTS

Structures and ionic states of tyrosine and tyrosinate are shown in Figure 1A. At pH 9, the tyrosine phenolic oxygen (pK_a ∼10) is protonated. The pK_a of the amino group has been reported to be ∼9.3.[34] Thus, at pH 9, tyrosine is present as a mixture of zwitterionic and anionic species. At pH 11, tyrosinate is a dianion, with negative charges on both the carboxylato group and the phenolate oxygen (pK_a ∼10). Deprotonation of the phenolic ring at pH 11 leads to a redshift of the S_1 and S_2 transitions (Figure 1B).

To study ET reactions on a picosecond time scale, a 280 nm pulse was used to photolyze tyrosinate or tyrosine samples in a dilute aqueous solution. In both cases, a neutral tyrosyl radical and a solvated electron were generated by photolysis. Therefore, photolysis was accompanied by ET at pH 11 and PCET at pH 9. Both species had detectable and distinguishable visible absorption bands (for example, see ref 30). Figure 2 shows time slices from multidimensional spectra (300−900 nm) acquired as a function of time after a 280 nm photoionizing flash from either tyrosine (blue) or tyrosinate (green) in solution. The signals are significant compared to a buffer background (Figure S2, SI). The time slices were derived from these tyrosine (blue) and tyrosinate (green) samples at 3, 15, 33, 113, 1073, and 2033 ps. The solvated electron is known to give rise to a broad absorptive band centered at 720 nm,[35] and the neutral tyrosyl radical gives rise to a narrow absorption band at 410 nm.[19] The spectra of the phenoxyl and tyrosyl cation radicals have been reported, and the spectra are distinguishable from those of the unprotonated neutral radical.[36,37] The pK_a of the tyrosyl cation radical is expected at −2.0[15] and is thus unlikely to be stable under the conditions employed here.

At pH 11 (Figure 2, green), the neutral tyrosyl radical and the solvated electron are fully formed at ∼3 ps, as monitored at 410 and 650 nm (Figure S3, SI), respectively. A band at 527 nm is also fully formed in 3 ps and is assigned to the S_1 excited state in agreement with the previous assignment of an ∼515 nm band to the S_1 excited state of phenolate.[30] The decay profile at 520 nm (Figure 3B, green) was fit with a multiexponential function (Table 1, Figure 3B, green), and a fast phase (19 ps, 49%) and a slow phase (580 ps, 22%) were derived. The derived 16−23 ps lifetime of the S_1 state agrees with an earlier report derived from phenolate.[30] In Figure 3A and C, the decay profiles of the neutral tyrosyl radical and the solvated electron

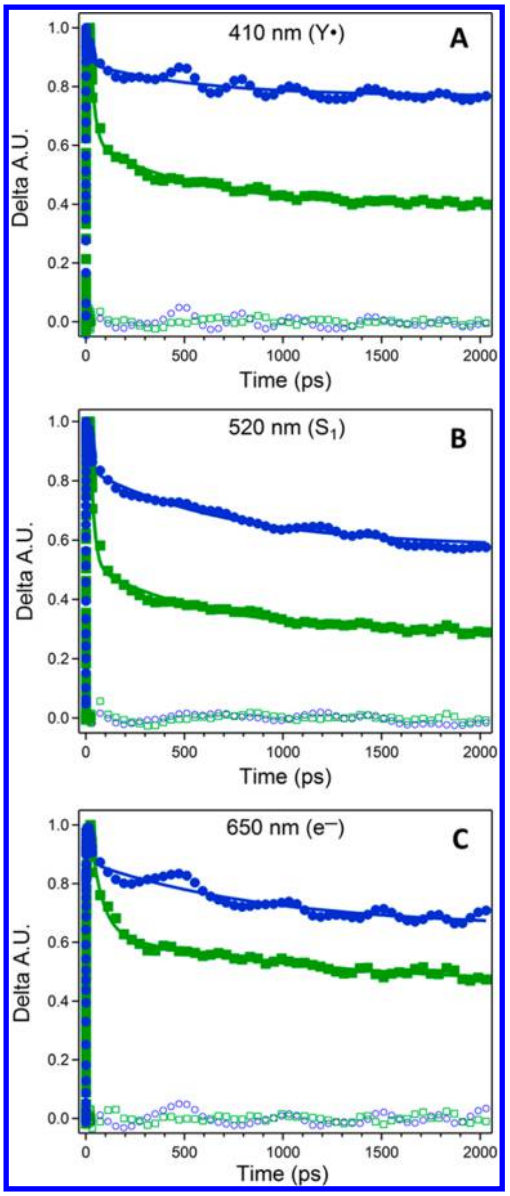

Figure 3. Comparison of kinetic transients in the picosecond to nanosecond range acquired after 280 nm photolysis of tyrosine at pH 9 (solid blue circles) or tyrosinate at pH 11 (solid green squares). The reaction at pH 9 corresponds to PCET, and the reaction at pH 11 corresponds to ET (Figure 1A). (A) Absorption of the neutral tyrosyl radical monitored at 410 nm. (B) Absorption of the S_1 excited state monitored at 520 nm. (C) Absorption of the solvated electron monitored at 650 nm. The solid lines are superimposed double exponential fits starting at 20 ps, and the open circles and squares are the corresponding residuals. Fitting parameters are presented in Table 1. The data were averaged from three independent measurements. The average data were normalized with respect to the maximum absorbance, which occurred at ∼2−3 ps at 410 and 520 nm and at ∼15 ps at 650 nm. Analyte concentration, 1 mM; buffer, 5 mM borate−NaOH.

were also fit with biexponential functions (Table 1) to derive lifetimes of 20−50 and 500−800 ps, respectively.

At pH 9, bands at 410 and 505 nm were also produced by photolysis and formed in ∼3 ps (Figures 2 and S3, SI, blue). The 505 nm band, which is prominent at 3 ps (Figure 2, blue), is assignable to the S_1 state of tyrosine. Although this band is blue-shifted with respect to the S_1 state band in tyrosinate, this

dx.doi.org/10.1021/jp510171z | J. Phys. Chem. B 2015, 119, 2726−2736

Table 1. Kinetic Parameters Obtained from Double Exponential[a] Fits to the Decay Profiles of Tyrosine, Tyrosinate, and Peptide A (pH 9 and 11)

	τ_1	A_1 (%)	τ_2	A_2 (%)	y_0 (%)	χ^2
			pH 9			
tyrosine						
410 nm	16 ± 6	0.08 (8)	910 ± 87	0.12 (12)	0.76 (80)	0.0140
520 nm	18 ± 2	0.14 (15)	1300 ± 150	0.31 (32)	0.50 (52)	0.0049
650 nm	14 ± 5	0.11 (11)	910 ± 190	0.22 (23)	0.65 (66)	0.0207
peptide A						
410 nm	16 ± 3	0.22 (30)	600 ± 37	0.29 (38)	0.24 (32)	0.0275
520 nm	14 ± 2	0.19 (25)	530 ± 20	0.31 (42)	0.25 (33)	0.0109
650 nm	13 ± 2	0.22 (26)	410 ± 35	0.23 (28)	0.39 (46)	0.0241
			pH 11			
tyrosinate						
410 nm	23 ± 2	0.38 (38)	500 ± 59	0.21 (21)	0.40 (40)	0.0117
520 nm	19 ± 1	0.49 (49)	580 ± 31	0.22 (22)	0.29 (29)	0.0121
650 nm	54 ± 7	0.34 (35)	820 ± 76	0.18 (18)	0.47 (47)	0.0186
peptide A						
410 nm	46 ± 6	0.36 (53)	980 ± 150	0.10 (15)	0.21 (31)	0.0221
520 nm	38 ± 6	0.34 (49)	720 ± 69	0.22 (31)	0.14 (20)	0.0297
650 nm	51 ± 10	0.36 (40)	1100 ± 140	0.22 (24)	0.32 (36)	0.0586

[a] $y = y_0 + A_1 \exp\{-(x - x_0)/\tau_1\} + A_2 \exp\{-(x - x_0)/\tau_2\}$; A = amplitude, τ = time constant (ps), x_0 = 20 ps. Transients were normalized with respect to the maximum absorbance in each averaged data set, which occurs at ∼2−3 ps at 410 and 520 nm and at ∼15 ps at 650 nm before fitting with Igor Pro 6.34A software (Wavemetrics Inc., Lake Oswego, OR).

blue shift is also observed in the ground state spectra (Figure 1B). Decay of the pH 9 S_1 signal was slower than the S_1 decay at pH 11. Biexponential fits at 520 nm gave time constants of 18 ps (15%) and 1300 ps (32%). There was also a significant nondecaying component required in the fit to the pH 9 data (52%). Overall, the lifetime of the signal assigned to the pH 9 S_1 state agrees with the reported 2−5 ns fluorescence lifetime of phenol and tyrosine in water.[38,39]

In addition to the 505 nm band, Figure 3 exhibits a 580 nm absorptive signal at pH 9, which was not observed at pH 11 (blue). The rise and decay times of the 580 and 520 nm signals were indistinguishable, suggesting that both signals arise from the S_1 excited state (Figure S4, SI). At pH 8, 280 nm photolysis generated primarily the 580 nm absorbing species (data not shown). This result suggests that the 580 nm signal arises from the S_1 excited state of the zwitterionic tyrosine species ($^+NH_3$), whereas the 520 nm band is assignable to the anionic form (NH_2) (Figure 1A). In previous work, the charges of the amino and carboxyl groups have been shown to alter the electronic properties of aromatic amino acids. For example, tyrosine fluorescence was reported to be pH dependent in the range from 0 to 9.[40] Note that a 600 nm band has been previously assigned to excimer formation in phenol−cyclohexane.[31] However, this is an unlikely explanation of the 580 nm band in our samples because of their low analyte concentration and the aqueous environment of the tyrosine.

At pH 9 (Figure 2, blue), the band at 350 nm, which grows in at ∼100 ps, can be assigned to interaction of the solvated electron with tyrosine. This band is not observed at pH 11 (Figure 2, green). In previous work, it was reported that this band was not significant in *p*-cresol, *p*-hydroxyphenylpropyl acetate, or tyrosine at pH 11.5 indicating that this secondary reaction is dependent on the charge and structure of phenol ring substituents.[38]

As observed for the S_1 signal, the rate of tyrosyl radical decay decreased at pH 9 compared to the rate at pH 11 (Figure 3, Table 1). At pH 9 (Figure 3A, blue), biexponential fits gave 16 ps (8%) and 910 ps (12%), with an appreciable nondecaying component (80%). The decay profile of the solvated electron, as monitored at 650 nm, was also biphasic in its decay and slower compared to that of pH 11 (Table 1, Figure 3C). Overall, the decay rates of the S_1 state, tyrosyl radical, and solvated electron correlated and increased as pH increased.

To evaluate the effect of the protein environment on picosecond reaction dynamics, 280 nm photolysis was conducted on peptide A samples at pH 9 and 11. Photolysis will oxidize Y5 (Figure 4A) and is expected to generate a neutral radical and a solvated electron.[27] The NMR derived structure[27] of peptide A is reproduced in Figures 4B and C. The NMR structure shows that Y5 interacts with a cross-strand histidine (H14) via a $\pi-\pi$ interaction (Figure 4C). The UV spectra of peptide A at pH 9 and 11 are compared to those of tyrosine and tyrosinate in Figures 4D and E, respectively. Observed differences at 200 nm reflect absorption from the peptide bond in the peptide A sample. However, the spectra of peptide A and tyrosine or tyrosinate solutions are similar in the 280 nm region. Previously, the pK_a of the Y5 phenolic oxygen was reported to be similar to the pK_a of tyrosine in solution.[27] In addition, an EPR signal from the neutral Y5 radical was generated by UV photolysis of peptide A at low temperature. Small changes in peak potential were observed when peptide A was compared to solution tyrosine, corresponding to shifts of less than 0.05 mV.[27] The peptide is folded at both pH 5 and 11, as assessed by NMR and CD measurements, respectively.

Using 280 nm photolysis, multidimensional transient absorption spectra (Figure S5, SI) were acquired on the picosecond time scale from peptide A. Time slices from experiments conducted at pH 9 (orange) and 11 (purple) are shown in Figure 5. The results are similar to the data acquired

dx.doi.org/10.1021/jp510171z | J. Phys. Chem. B 2015, 119, 2726−2736

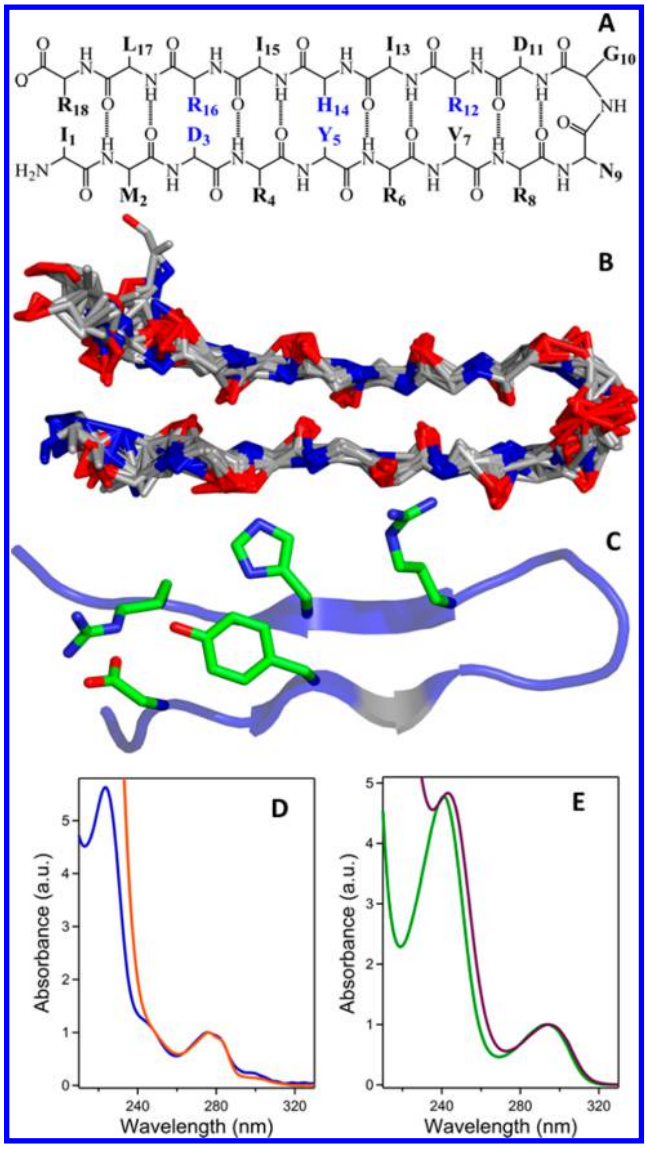

Figure 4. (A) Primary sequence of peptide A (IMDRYRVRNGDR-IHIRLR). (B) β-Hairpin backbone of peptide A, as derived from the 20 lowest energy NMR structures. (C) Cross-strand interactions of Y5 in peptide A. (D) Comparison of steady state absorption spectra of a 1 mM solution of tyrosine (blue) with peptide A (orange) at pH 9, which were normalized with respect to the absorption of tyrosine at 276 nm ($S_1 \leftarrow S_0$ transition of tyrosine). (E) Comparison of steady state absorption spectra of a 1 mM solution of tyrosinate (green) with peptide A (purple) at pH 11, which were normalized with respect to the absorption of tyrosinate at 294 nm ($S_1 \leftarrow S_0$ transition of tyrosinate).

from solution tyrosine and tyrosinate (Figure 2). Note that both the ~520 and ~580 nm S_1 signals are observed in peptide A at pH 9. The only group titrating between pH 8 and 11 is the peptide's amino terminal group. Therefore, we attribute the 580 nm band to the S_1 excited state in the peptide in which the amino terminus is protonated (Figure 1A).

In peptide A samples, formation of the tyrosyl radical and the 520 nm excited state is complete in 3 ps (Figure S6, SI), which was also observed for solution tyrosine and tyrosinate. Figure 6 shows decay profiles for three species in peptide A: the tyrosyl radical (A, 410 nm), the S_1 excited state (B, 520 nm), and the solvated electron (C, 650 nm). Data were acquired at either pH 9 (orange) or 11 (purple). The 410 nm profiles derived from tyrosinate (green) and tyrosine (blue) are reproduced from Figure 3 as dashed and dotted lines in Figure 6. The peptide data are shown with double exponential fits superimposed (see parameters in Table 1). Significantly, at both pH values, the neutral tyrosyl radical (Figure 6A), the S_1 state decay (Figure 6B), and the decay of the solvated electron (Figure 6C) were accelerated in the peptide compared to those of solution samples at the same pH.

To determine if noncovalent interactions between tyrosinate and histidine in solution can cause this rate acceleration, multidimensional spectra were recorded from an equimolar mixture of tyrosine and histidine at pH 11 (Figure S7, SI). The spectra were similar to those acquired from tyrosinate alone (Figure 2). Superposition of the decay profiles at 410, 520, and 650 nm showed that the decay rates in tyrosinate (green) and in the tyrosinate/histidine mixture (violet) were indistinguishable from each other (Figure S8, SI). Signals in the peptide A sample exhibited more rapid decay at all three wavelengths (Figure S8, SI). We conclude that rate acceleration in the peptide is due to the influence of covalent bonding or specific interactions, such as cross-strand hydrogen bonding or the $\pi-\pi$ interaction between H14 and Y5.

DISCUSSION

In this report, the formation and decay kinetics of the tyrosyl radical, the S_1 excited state, and the solvated electron were monitored on the picosecond time scale after 280 nm photolysis of solution tyrosine and tyrosinate. These kinetics and time-resolved spectra were compared to data derived from peptide A. The multidimensional spectra were similar when the peptide A and solution samples were compared. The neutral tyrosyl radical, the S_1 excited state, and the solvated electron were fully formed in less than or equal to 6 ps in all samples at pH 9 and 11. These data demonstrate that photoexcitation at 280 nm results in rapid OH bond cleavage in tyrosine and peptide A at pH 9 (PCET) and results in rapid ET from the excited S_1 state at pH 11.

In tyrosinate at pH 11, the 410 nm decay profile of the tyrosyl radical signal was analyzed and lifetimes of ~20 and 500 ps were derived. At pH 9 (tyrosine), two phases were also derived, but the amplitudes and lifetimes were changed relative to those of the pH 11 samples. Multiexponential decay profiles at both pH values may be related to a pH-induced change in the distribution of tyrosyl radical conformers in solution. These conformers are described by differences in ring dihedral and backbone dihedral angle, and the distribution and relative energies have been shown to be sensitive to protonation/deprotonaton of the terminal carboxylate group.[41] The ET decay profile is biphasic even in peptide A, which might have been expected to have a conformational distribution different from that of solution tyrosine and tyrosinate.

When tyrosinate (pH 11) is compared to tyrosine (pH 9), the decay profiles are consistent with an overall slowing of the rate of the S_1 excited state and decay of the tyrosyl radical and solvated electron. pH dependence was also observed in the decay of tyrosyl radicals at pH 5 (k_{obs} = 420 s^{-1}) and pH 8.5 (~5.4 × 10^4 s^{-1}), when produced by sensitization of aqueous solutions with $[Ru(bpy)_3]^{2+}$ (ref 26, but see also ref 40). The kinetic correlations reported in Table 1 are consistent with a mechanism in which the tyrosyl radical and the solvated electron recombine at both pH values.

To evaluate the cause of the rate reduction at low pH, three possible mechanisms for PCET are considered (Figure 7A). In

dx.doi.org/10.1021/jp510171z | J. Phys. Chem. B 2015, 119, 2726−2736

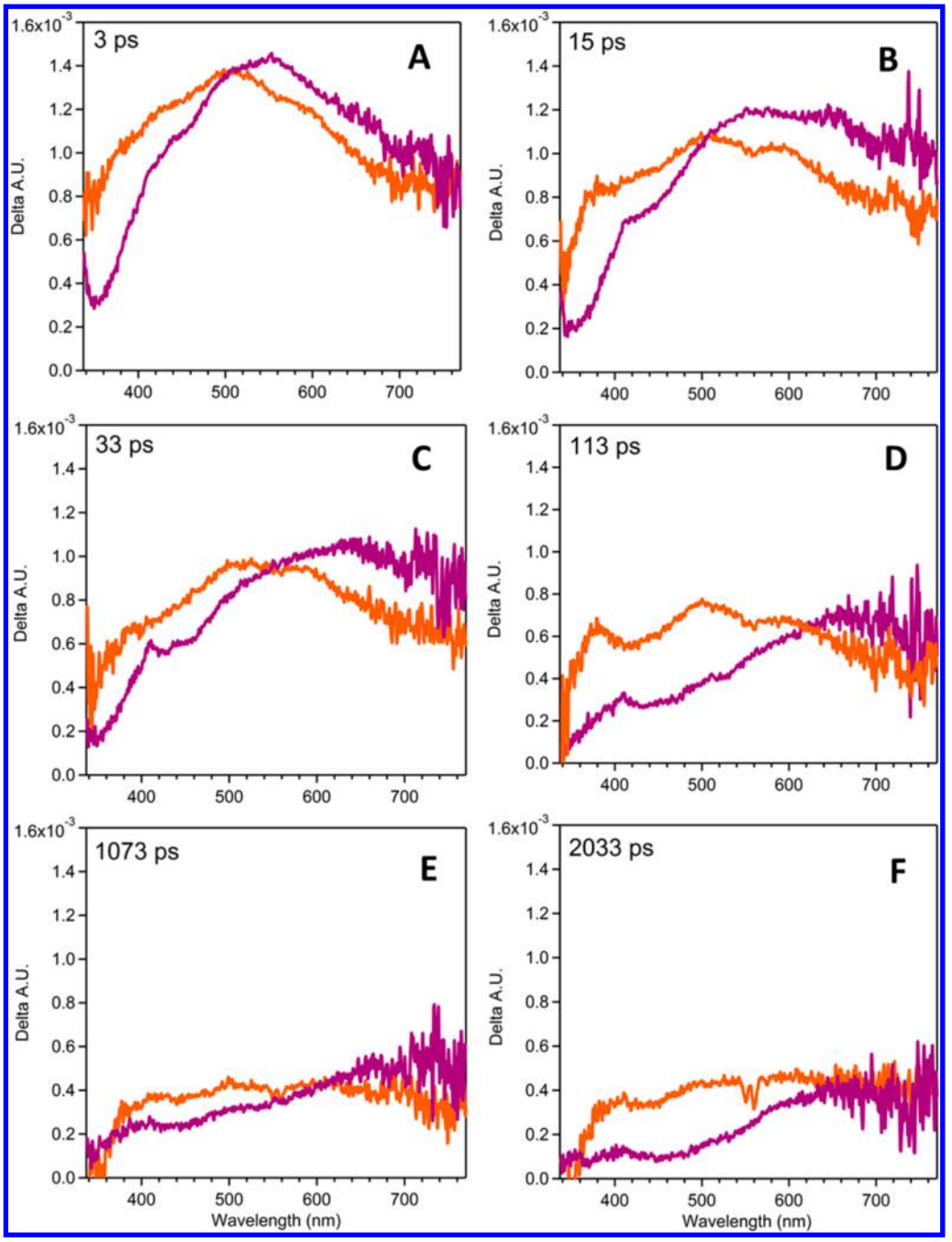

Figure 5. Spectral slices derived from peptide A at either pH 9 (orange) or 11 (purple) at the indicated time points. Analyte concentration, 1 mM; buffer, 5 mM borate−NaOH.

the middle pathway, PT and ET occur simultaneously without the formation of an intermediate (CPET). In the top stepwise pathway, ET proceeds first to form a tyrosinate species, which is then protonated to give tyrosine (ETPT). In the bottom stepwise pathway, PT proceeds first to form a tyrosyl cation radical, which is then reduced to form tyrosine (PTET). In these two paths, either PT or ET may be rate limiting. Our observation that decreasing pH reduces the rate of the reaction may suggest that PT is not rate limiting. However, further experiments are necessary to address this point.

A PTET mechanism (Figure 7A, bottom) is not expected in these experiments. Tyrosyl cation radicals have a low pK_a, are unstable in aqueous solution, and if produced would have been spectroscopically distinct from the 410 nm band of the neutral tyrosyl radical.[15,36,37] The other mechanisms for PCET at pH 9 are represented in Figure 7B. The top reaction illustrates a two-step ETPT mechanism. If ET is assumed to be the rate-limiting step, this reaction corresponds to slow formation of the tyrosinate anion and then rapid protonation to form tyrosine (Figure 7B). In this context, k_{ET} must be pH dependent to explain the observed pH dependence.

$$\log k_{ET} = 13 - \frac{\beta}{2.303}(R - 3.6) - 3.1\left[\frac{(\Delta G^\circ + \lambda)^2}{\lambda}\right] \quad (3)$$

To evaluate factors that could influence k_{ET} in an ETPT mechanism, Dutton's ruler[1] (eq 3) was employed. This

dx.doi.org/10.1021/jp510171z | J. Phys. Chem. B 2015, 119, 2726−2736

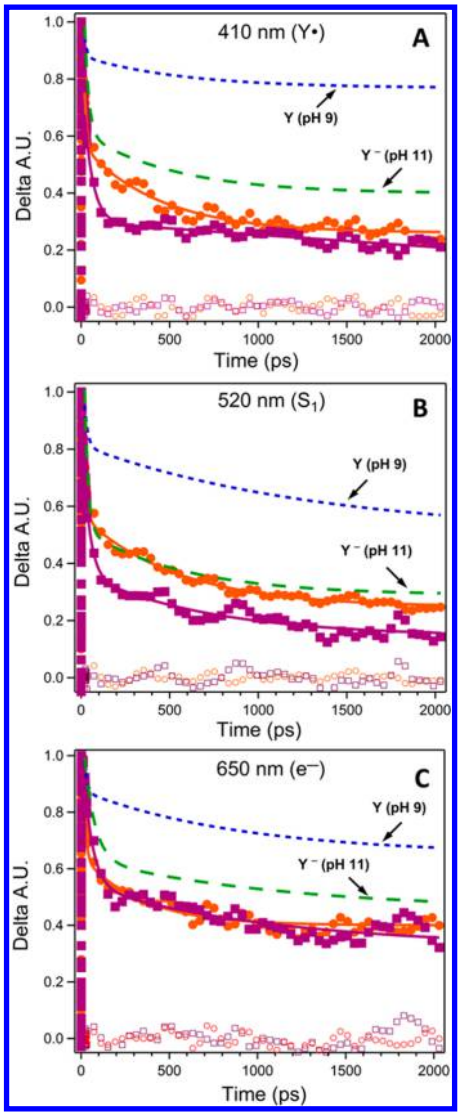

Figure 6. Comparison of kinetic transients in the picosecond to nanosecond range, acquired after 280 nm photolysis of peptide A at pH 9 (solid orange circles) and pH 11 (solid purple squares). Kinetics at pH 9 correspond to PCET, and those at pH 11 correspond to ET (Figure 1A). (A) Absorption of the neutral tyrosyl radical monitored at 410 nm. (B) Absorption of the S_1 excited state monitored at 520 nm. (C) Absorption of the solvated electron monitored at 650 nm. The solid lines are superimposed double exponential fits starting at 20 ps, and the open circles and squares are the corresponding residuals. Fitting parameters are presented in Table 1. The data were averaged from three independent measurements. The averaged data were normalized with respect to the maximum absorbance, which occurred at ~2−3 ps at 410 and 520 nm and at ~15 ps at 650 nm. Analyte concentration, 1 mM; buffer, 5 mM borate−NaOH. The dashed and dotted blue and green lines are reproduced from Figure 3 and show the corresponding decay profiles for tyrosinate (green) and tyrosine (blue).

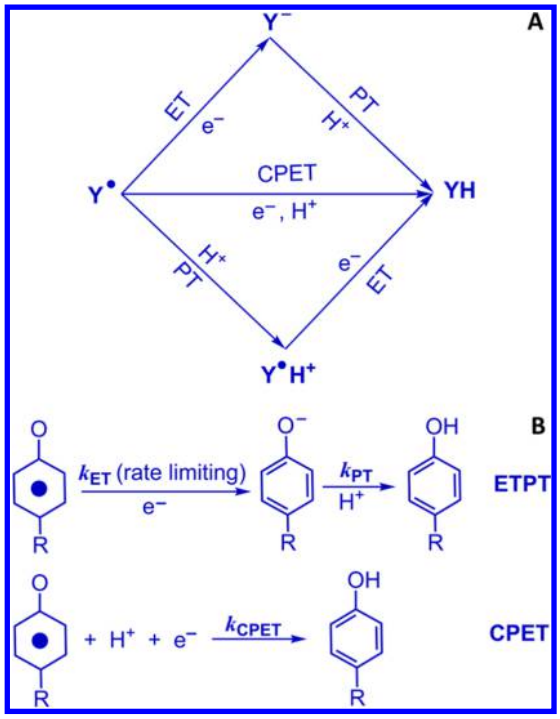

Figure 7. (A) Overview of PCET mechanisms for tyrosyl radical decay, corresponding to stepwise ETPT (top), concerted PT and ET (CPET, middle), or stepwise PTET (bottom). In ETPT and PTET, either ET or PT may be rate limiting. (B) ETPT (ET rate limiting) and CPET mechanisms, which can account for the pH dependence and transient absorption results reported here.

expression was derived from fits to empirical data (eq 1) and is useful as a first approximation in predicting the rate of electron transfer k_{ET}.[42] In using eq 3, recombination between the tyrosyl radical and solvated electron is assumed to be the major pathway of decay. The reorganization energy (λ, eV), driving force ($\Delta G°$, eV), distance (R, Å), and electronic coupling (β, Å^{-1}) are variables in eq 3. This equation assumes an optimal, activation-less rate of 10^{13} s^{-1} at a van der Waals contact of 3.6 Å. The value of 3.1 was empirically derived, collects room temperature constants, and has been validated in studies of photosynthetic electron transfer (reviewed in refs 42 and 43). To use Dutton's ruler, the values of the driving force were estimated from the reported midpoint potentials of tyrosine and tyrosinate (pH 9, 0.72 eV; pH 11, 0.67 eV).[13] The reorganization energy was assumed to be 1 eV[1] and pH independent. The β factor was taken from the literature as 1.55 Å^{-1}, which corresponds to the value derived from aqueous glasses.[44] The distance between the solvated electron and tyrosyl radical is not known. Assuming a distance of 9 Å, ET rates qualitatively similar to the experimentally derived values were predicted: 1.3×10^9 s^{-1} (τ = 750 ps) for tyrosine and 1.1×10^9 s^{-1} (τ = 940 ps) for tyrosinate. Thus, the change in midpoint potential suggests an increased rate at pH 9. However, a decrease in rate is observed experimentally. Therefore, a change in midpoint potential alone cannot explain our results. A pH-induced change in conformational distribution or solvent reorganization energy could account for a change in k_{ET}. However, to be consistent with ETPT, the conformational distribution or solvent reorganization in peptide A samples must exhibit a similar pH dependence.

The bottom reaction in Figure 7B is a one-step, concerted PT and ET (CPET) reaction, which is also a possible mechanism for the recombination of the tyrosyl radical and solvated electron at pH 9. A CPET reaction can readily explain the slower rate at pH 9 because CPET reactions are associated with higher reorganization energies compared to those of non-CPET mechanisms at pH 11.[45] For example, a value of 2 eV for tyrosine-based CPET has been reported.[22,23] A change from 1 to 2 eV would slow the ET rate by approximately 2 orders of magnitude compared to a reorganization energy of 1 eV using

dx.doi.org/10.1021/jp510171z | J. Phys. Chem. B 2015, 119, 2726−2736

the parameters outlined above. Therefore, modest changes in reorganization energy could account for the decrease in rate observed in our experiments at pH 9.

Previously, the formation and decay of tyrosyl radicals have been monitored in model compounds, but on longer (microsecond) time scales using photosensitizers. At pH values below the pK_a of tyrosine, the rate constant for intramolecular electron transfer from tyrosine to covalently linked ruthenium increased as pH increased.[22,23] The rates were determined by monitoring the recovery of ruthenium ground state absorption (450 nm) and the absorption of the quencher methyl viologen at 600 nm. The reorganization energy λ was determined to be ~2 eV. It was concluded that these results were consistent with a CPET mechanism. At pH greater than 10, the ET rate increased 100-fold, and λ decreased to 0.9 eV. These experimental results were reproduced in subsequent theoretical calculations.[46] The pH dependence and reorganization energies, which are characteristic of CPET reactions, have been discussed extensively in other studies. CPET has been shown to be facilitated by hydrogen bonding and to be mediated by water (for examples, see refs 45 and 47−52). For example, decay of the YZ radical in PSII exhibits no pH dependence compared to the slower decay of the YD radical. This difference was attributed to extensive hydrogen bonding of YZ and a resulting CPET mechanism for YZ radical decay.[53−56]

In a recent study on the α-helical model peptide α3, its Y32 radical was generated using the photosensitizer $[Ru(bpy)_3]^{2+}$, and formation and decay reactions were monitored on a microsecond to second time scale. A CPET or PTET mechanism for the oxidation reaction was inferred based on the pH and solvent isotope dependence of the oxidation rate. Decay of the Y32 radical was many orders of magnitude slower than that of the tyrosyl radical in solution. This slow decay, on a second time scale, is consistent with a hydrophobic environment for Y32.[26]

In contrast to that of α3, the tyrosyl radical decay in peptide A occurs on the picosecond time scale, which is the same order of magnitude as the tyrosyl radical in solution. This difference is attributed to the aqueous, hydrogen-bonding environment of Y5 in peptide A. Significantly, upon comparison of peptide A and tyrosine/tyrosinate, an ~2-fold increase in Y5 radical decay rate is measured in the peptide. This increase was observed both at pH 9 and 11. When compared to tyrosine/tyrosinate, other amino acid side chains in peptide A, such as histidine and methionine, are more difficult to oxidize and are not expected to participate in a charge relay mechanism.[57] For example, the midpoint potential of methionine has been reported to be 1.7 V versus that of NHE.[58] In addition, the peak potential of Y5 is similar to that of solution tyrosine and tyrosinate, and the UV−vis spectrum of Y5 is similar to that of solution samples.[27] The 2-fold increase in rate might be attributable to a change in β, which describes the distance dependence of electronic coupling in a tunneling mechanism. Electronic coupling depends on the nature of the intervening medium. It has been reported that β is 1.55 $Å^{-1}$ in an aqueous glass and decreases to 1.1 $Å^{-1}$ when ET is mediated through a β-strand.[44] Electronic coupling in proteins and peptides is dependent on secondary structure[59] and conformation[60,61] and has been shown to increase in a β-turn to form a depsipeptide.[62] Dutton's ruler (eq 3) can be used to estimate the value of β, which would give a 2-fold increased rate in peptide A. Using the midpoint potential at pH 9 as an estimate of driving force (0.72 eV), a reorganization energy of 1 eV, and a distance of 9 Å, this analysis predicts a β of 1.4 $Å^{-1}$ in peptide A. This is a value previously deduced to be characteristic of tunneling in proteins.[1] However, the 2-fold increase in rate could also be due to specific, noncovalent interactions in the peptide, such as the $\pi-\pi$ interaction between H14 and Y5. Future experiments on peptide sequence variants will address this point.

In conclusion, we show that 280 nm photolysis leads to picosecond PCET and ET reactions in tryosine and tyrosinate, respectively. A neutral radical is formed in 3 ps in peptide A at either pH 9 or 11. Further, decreasing pH slows the rate of tyrosyl radical decay. This rate change is observed both in solution and in the peptide. The pH 9 mechanism can be explained by either a stepwise ETPT mechanism or a CPET mechanism. Also, we show that picosecond ET and PCET reactions are accelerated by coupling through covalent and specific noncovalent interactions, such as hydrogen bonding and $\pi-\pi$ interactions, in the peptide. This result has important implications in understanding the rapid ET and PCET reactions of photosynthesis and DNA photolyase, which are likely to be accelerated by such targeted interactions with the redox-active amino acid.

■ ASSOCIATED CONTENT

Supporting Information

UV spectra of samples before and after 280 nm photolysis measurements, kinetic profiles, and multidimensional spectra derived from tyrosine, tyrosinate, peptide A, and tyrosine/histidine mixtures. This material is available free of charge via the Internet at http://pubs.acs.org.

■ AUTHOR INFORMATION

Corresponding Author

*E-mail: bridgette.barry@chemistry.gatech.edu.

Notes

The authors declare no competing financial interest.

■ ACKNOWLEDGMENTS

This research was funded by NSF CLP 12-13350 (B.A.B.). B.A.B. is grateful to Prof. Olof Einarsdottir and her research group for interesting discussions.

■ REFERENCES

(1) Moser, C. C.; Keske, J. M.; Warncke, K.; Farid, R. S.; Dutton, P. L. Nature of Biological Electron Transfer. *Nature* **1992**, *355*, 796−802.

(2) Dempsey, J. L.; Winkler, J. R.; Gray, H. B. Proton-Coupled Electron Flow in Protein Redox Machines. *Chem. Rev.* **2010**, *110*, 7024−7039.

(3) Lukacs, A.; Eker, A. P.; Byrdin, M.; Brettel, K.; Vos, M. H. Electron Hopping through the 15 Å Triple Tryptophan Molecular Wire in DNA Photolyase Occurs within 30 ps. *J. Am. Chem. Soc.* **2008**, *130*, 14394−14395.

(4) Whittaker, M. M.; Whittaker, J. W. Tyrosine-Derived Free Radical in Apogalactose Oxidase. *J. Biol. Chem.* **1990**, *265*, 9610−9613.

(5) Lu, J. M.; Rogge, C. E.; Wu, G.; Kulmacz, R. J.; van der Donk, W. A.; Tsai, A. L. Cyclooxygenase Reaction Mechanism of PGHS–Evidence for a Reversible Transition between a Pentadienyl Radical and a New Tyrosyl Radical by Nitric Oxide Trapping. *J. Inorg. Biochem.* **2011**, *105*, 356−365.

(6) Gupta, A.; Mukherjee, A.; Matsui, K.; Roth, J. P. Evidence for Protein Radical-Mediated Nuclear Tunneling in Fatty Acid α-Oxygenase. *J. Am. Chem. Soc.* **2008**, *130*, 11274−11275.

(7) Zhao, X.; Suarez, J.; Khajo, A.; Yu, S.; Metlitsky, L.; Magliozzo, R. S. A Radical on the Met-Tyr-Trp Modification Required for Catalase

Activity in Catalase-Peroxidase is Established by Isotopic Labeling and Site-Directed Mutagenesis. *J. Am. Chem. Soc.* **2010**, *132*, 8268−8269.
(8) Barry, B. A. Proton Coupled Electron Transfer and Redox Active Tyrosines in Photosystem II. *J. Photochem. Photobiol., B* **2011**, *104*, 60−71.
(9) Minnihan, E. C.; Nocera, D. G.; Stubbe, J. Reversible, Long-Range Radical Transfer in *E. coli* Class Ia Ribonucleotide Reductase. *Acc. Chem. Res.* **2013**, *46*, 2524−2535.
(10) Umena, Y.; Kawakami, K.; Shen, J.-R.; Kamiya, N. Crystal Structure of Oxygen-Evolving Photosystem II at a Resolution of 1.9 Å. *Nature* **2011**, *473*, 55−60.
(11) Martin, R. B.; Edsall, J. T.; Wetlaufer, D. B.; Hollingworth, B. R. A Complete Ionization Scheme for Tyrosine, and the Ionization Constants of Some Tyrosine Derivatives. *J. Biol. Chem.* **1958**, *233*, 1429−1435.
(12) Marcus, R. A. Electron Transfer Reactions in Chemistry: Theory and Experiment. *Pure Appl. Chem.* **1997**, *69*, 13−29.
(13) Harriman, A. Further Comments on the Redox Potentials of Tryptophan and Tyrosine. *J. Phys. Chem.* **1987**, *91*, 6102−6104.
(14) Wenger, O. S.; Leigh, B. S.; Villahermosa, R. M.; Gray, H. B.; Winkler, J. R. Electron Tunneling through Organic Molecules in Frozen Glasses. *Science* **2005**, *307*, 99−102.
(15) Dixon, W. T.; Murphy, D. Determination of the Acidity Constants of Some Phenol Radical Cations by Means of Electron Spin Resonance. *J. Chem. Soc., Faraday Trans. 2* **1976**, *72*, 1221−1230.
(16) Weinberg, D. R.; Gagliardi, C. J.; Hull, J. F.; Murphy, C. F.; Kent, C. A.; Westlake, B. C., II; Paul, A.; Ess, D. H.; McCafferty, D. G.; Meyer, T. J. Proton-Coupled Electron Transfer. *Chem. Rev.* **2012**, *112*, 4016−4093.
(17) Reece, S. Y.; Hodgkiss, J. M.; Stubbe, J.; Nocera, D. G. Proton-Coupled Electron Transfer: The Mechanistic Underpinning for Radical Transport and Catalysis in Biology. *Philos. Trans. R. Soc., B* **2006**, *361*, 1351−1364.
(18) Hammes-Schiffer, S.; Soudackov, A. V. Proton-Coupled Electron Transfer in Solution, Proteins, and Electrochemistry. *J. Phys. Chem. B* **2008**, *112*, 14108−14123.
(19) Bent, D. V.; Hayon, E. Excited State Chemistry of Aromatic Amino Acids and Related Peptides. I. Tyrosine. *J. Am. Chem. Soc.* **1975**, *97*, 2599−2606.
(20) Cappuccio, J. A.; Ayala, I.; Elliot, G. I.; Szundi, I.; Lewis, J.; Konopelski, J. P.; Barry, B. A.; Einarsdóttir, Ó. Modeling the Active Site of Cytochrome Oxidase: Synthesis and Characterization of a Cross-Linked Histidine-Phenol. *J. Am. Chem. Soc.* **2002**, *124*, 1750−1760.
(21) Reece, S. Y.; Stubbe, J.; Nocera, D. G. pH Dependence of Charge Transfer between Tryptophan and Tyrosine in Dipeptides. *Biochim. Biophys. Acta* **2005**, *1706*, 232−238.
(22) Sjödin, M.; Styring, S.; Akermark, B.; Sun, L.; Hammarström, L. The Mechanism for Proton-Coupled Electron Transfer from Tyrosine in a Model Complex and Comparisons with Y_z Oxidation in Photosystem II. *Philos. Trans. R. Soc., B* **2002**, *357*, 1471−1478.
(23) Sjödin, M.; Styring, S.; Akermark, B.; Sun, L.; Hammarström, L. Proton-Coupled Electron Transfer from Tyrosine in a Tyrosine-Ruthenium-Tris-Bipyridine Complex: Comparison with Tyrosine Z Oxidation in Photosystem II. *J. Am. Chem. Soc.* **2000**, *122*, 3932−3936.
(24) Shih, C.; Museth, A. K.; Abrahamsson, M.; Blanco-Rodriguez, A. M.; Di Bilio, A. J.; Sudhamsu, J.; Crane, B. R.; Ronayne, K. L.; Towrie, M.; Vlček, A., Jr.; et al. Tryptophan-Accelerated Electron Flow through Proteins. *Science* **2008**, *320*, 1760−1762.
(25) Warren, J. J.; Winkler, J. R.; Gray, H. B. Redox Properties of Tyrosine and Related Molecules. *FEBS Lett.* **2012**, *586*, 596−602.
(26) Glover, S. D.; Jorge, C.; Liang, L.; Valentine, K. G.; Hammarstrom, L.; Tommos, C. Photochemical Tyrosine Oxidation in the Structurally Well-Defined α3Y Protein: Proton-Coupled Electron Transfer and a Long-Lived Tyrosine Radical. *J. Am. Chem. Soc.* **2014**, *136*, 14039−14051.
(27) Sibert, R. S.; Josowicz, M.; Porcelli, F.; Veglia, G.; Range, K.; Barry, B. A. Proton-Coupled Electron Transfer in Biomimetic Peptide as a Model of Enzyme Regulatory Mechanism. *J. Am. Chem. Soc.* **2007**, *129*, 4393−4400.
(28) Sibert, R. S.; Josowicz, M.; Barry, B. A. Control of Proton and Electron Transfer in de Novo Designed, Biomimetic Beta Hairpins. *ACS Chem. Biol.* **2010**, *5*, 1157−1168.
(29) Gerken, S.; Brettel, K.; Schlodder, E.; Witt, H. T. Optical Characterization of the Immediate Donor to Chlorophyll a_{II}^{+} in O_2-Evolving Photosystem II Complexes. *FEBS Lett.* **1988**, *237*, 69−75.
(30) Chen, X.; Larsen, D. S.; Bradforth, S. E.; van Stokkum, I. H. Broadband Spectral Probing Revealing Ultrafast Photochemical Branching after Ultraviolet Excitation of the Aqueous Phenolate Anion. *J. Phys. Chem. A* **2011**, *115*, 3807−3819.
(31) Zhang, Y. Y.; Oliver, T. A. A.; Ashfold, M. N. R.; Bradforth, S. E. Contrasting the Excited State Reaction Pathways of Phenol and Para-Methylthiophenol in the Gas and Liquid Phases. *Faraday Discuss.* **2012**, *157*, 141−163.
(32) Chaudhry, A. F.; Verma, M.; Morgan, M. T.; Henary, M. M.; Siegel, N.; Hales, J. M.; Perry, J. W.; Fahrni, C. J. Kinetically Controlled Photoinduced Electron Transfer Switching in Cu(I)-Responsive Fluorescent Probes. *J. Am. Chem. Soc.* **2010**, *132*, 737−747.
(33) Kovalenko, S. A.; Dobryakov, A. L.; Ruthmann, J.; Ernsting, N. P. Femtosecond Spectroscopy of Condensed Phases with Chirped Supercontinuum Probing. *Phys. Rev. A* **1999**, *59*, 2369−2384.
(34) Edsall, J. T.; Martin, R. B.; Hollingworth, B. R. Ionization of Individual Groups in Dibasic Acids, with Application to the Amino and Hydroxyl Groups of Tyrosine. *Proc. Natl. Acad. Sci. U.S.A.* **1958**, *44*, 505−518.
(35) Buxton, G. V.; Greenstock, C. L.; Helman, W. P.; Ross, A. B. Critical Review of Rate Constants for Reactions of Hydrated Electrons, Hydrogen Atoms and Hydroxyl Radicals ($^{\bullet}OH/^{\bullet}O^{-}$) in Aqueous Solution. *J. Phys. Chem. Ref. Data* **1988**, *17*, 513−886.
(36) Baugher, J. F.; Grossweiner, L. I. Photolysis Mechanism of Aqueous Tyrosine and Tyrosyl Peptides. *Photochem. Photobiol.* **1978**, *28*, 175−184.
(37) Ganapathi, M. R.; Hermann, R.; Naumov, S.; Brede, O. Free Electron Transfer from Several Phenols to Radical Cations of Non-Polar Solvents. *Phys. Chem. Chem. Phys.* **2000**, *2*, 4947−4955.
(38) Feitelson, J.; Hayon, E. Electron Ejection and Electron Capture by Phenolic Compounds. *J. Phys. Chem.* **1973**, *77*, 10−15.
(39) Hermann, R.; Mahalaxmi, G. R.; Jochum, T.; Naumov, S.; Brede, O. Balance of the Deactivation Channels of the First Excited Singlet State of Phenols: Effect of Alkyl Substitution, Sterical Hindrance, and Solvent Polarity. *J. Phys. Chem. A* **2002**, *106*, 2379−2389.
(40) Feitelson, J. On the Mechanism of Fluorescence Quenching. Tyrosine and Similar Compounds. *J. Phys. Chem.* **1964**, *68*, 391−397.
(41) Offenbacher, A. R.; Burns, L. A.; Sherrill, C. D.; Barry, B. A. Redox-Linked Conformational Control of Proton-Coupled Electron Transfer: Y122 in the Ribonucleotide Reductase β2 Subunit. *J. Phys. Chem. B* **2013**, *117*, 8457−8468.
(42) Crofts, A. R.; Rose, S. Marcus Treatment of Endergonic Reactions: A Commentary. *Biochim. Biophys. Acta* **2007**, *1767*, 1228−1232.
(43) Page, C.; Moser, C.; Chen, X.; Dutton, P. Natural Engineering Principles of Electron Tunnelling in Biological Oxidation-Reduction. *Nature* **1999**, *402*, 47−52.
(44) Gray, H. B.; Winkler, J. R. Long-Range Electron Transfer. *Proc. Natl. Acad. Sci. U.S.A.* **2005**, *102*, 3534−3539.
(45) Rhile, I. J.; Markle, T. F.; Nagao, H.; DiPasquale, A. G.; Lam, O. P.; Lockwood, M. A.; Rotter, K.; Mayer, J. M. Concerted Proton-Electron Transfer in the Oxidation of Hydrogen Bonded Phenols. *J. Am. Chem. Soc.* **2006**, *128*, 6075−6088.
(46) Carra, C.; Iordanova, N.; Hammes-Schiffer, S. Proton-Coupled Electron Transfer in a Model for Tyrosine Oxidation in Photosystem II. *J. Am. Chem. Soc.* **2003**, *125*, 10429−10436.
(47) Rhile, I. J.; Mayer, J. M. One-Electron Oxidation of a Hydrogen-Bonded Phenol Occurs by Concerted Proton-Coupled Electron Transfer. *J. Am. Chem. Soc.* **2004**, *126*, 12718−12719.

(48) Sjödin, M.; Irebo, T.; Utas, J. E.; Lind, J.; Merényi, G.; Akermark, B.; Hammarström, L. Kinetic Effects of Hydrogen Bonds on Proton-Coupled Electron Transfer from Phenols. *J. Am. Chem. Soc.* **2006**, *128*, 13076−13083.
(49) Irebo, T.; Reece, S. Y.; Sjödin, M.; Nocera, D. G.; Hammarström, L. Proton-Coupled Electron Transfer of Tyrosine Oxidation: Buffer Dependence and Parallel Mechanisms. *J. Am. Chem. Soc.* **2007**, *129*, 15462−15464.
(50) Bonin, J.; Costentin, C.; Louault, C.; Robert, M.; Routier, M.; Savéant, J.-M. Intrinsic Reactivity and Driving Force Dependence in Concerted Proton-Electron Transfers to Water Illustrated by Phenol Oxidation. *Proc. Natl. Acad. Sci. U.S.A.* **2010**, *107*, 3367−3372.
(51) Bonin, J.; Costentin, C.; Louault, C.; Robert, M.; Saveant, J. M. Water (in Water) as an Intrinsically Efficient Proton Acceptor in Concerted Proton Electron Transfers. *J. Am. Chem. Soc.* **2011**, *133*, 6668−6674.
(52) Bonin, J.; Costentin, C.; Robert, M.; Saveant, J. M.; Tard, C. Hydrogen-Bond Relays in Concerted Proton-Electron Transfers. *Acc. Chem. Res.* **2012**, *45*, 372−381.
(53) Jenson, D.; Evans, A.; Barry, B. A. Proton-Coupled Electron Transfer and Tyrosine D of Photosystem II. *J. Phys. Chem. B* **2007**, *111*, 12599−12604.
(54) Jenson, D.; Barry, B. A. Proton-Coupled Electron Transfer in Photosystem II: Proton Inventory of a Redox Active Tyrosine. *J. Am. Chem. Soc.* **2009**, *131*, 10567−10573.
(55) Keough, J.; Jenson, D. L.; Zuniga, A.; Barry, B. A. Proton Coupled Electron Transfer and Redox-Active Tyrosine Z in the Photosynthetic Oxygen Evolving Complex. *J. Am. Chem. Soc.* **2011**, *133*, 11084−11087.
(56) Keough, J.; Zuniga, A.; Jenson, D. L.; Barry, B. A. Redox Control and Hydrogen Bonding Networks: Proton-Coupled Electron Transfer Reactions and Tyrosine Z in the Photosynthetic Oxygen-Evolving Complex. *J. Phys. Chem. B* **2013**, *117*, 1296−1307.
(57) Brabec, V.; Mornstein, V. Electrochemical Behavior of Proteins at Graphite Electrodes: II. Electrooxidation of Amino Acids. *Biophys. Chem.* **1980**, *12*, 159−165.
(58) Wang, M.; Gao, J.; Muller, P.; Giese, B. Electron Transfer in Peptides with Cysteine and Methionine as Relay Amino Acids. *Angew. Chem., Int. Ed.* **2009**, *48*, 4232−4334.
(59) Beratan, D. N.; Onuchic, J. N.; Betts, J. N.; Bowler, B. E.; Gray, H. B. Electron-Tunneling Pathway in Ruthenated Proteins. *J. Am. Chem. Soc.* **1990**, *112*, 7915−7921.
(60) Issa, J. B.; Salameh, A. S.; Castner, E. W., Jr.; Wishart, J. F.; Isied, S. S. Conformational Analysis of the Electron-Transfer Kinetics across Oligoproline Peptides Using *N*,*N*-Dimethyl-1,4-Benzenediamine Donors and Pyrene-1-Sulfonyl Acceptors. *J. Phys. Chem. B* **2007**, *111*, 6878−6886.
(61) Issa, J. B.; Krogh-Jespersen, K.; Isied, S. S. Conformational Dependence of Electronic Coupling across Peptide Bonds: A Ramanchandran Map. *J. Phys. Chem. C* **2010**, *114*, 20809−20812.
(62) Williamson, D. A.; Bowler, B. E. Electron Transfer through the Hydrogen-Bonded Interface of a β-Turn-Forming Depsipeptide. *J. Am. Chem. Soc.* **1998**, *120*, 10902−10911.